ELSEVIER

International Journal of Solids and Structures 41 (2004) 3653–3674

INTERNATIONAL JOURNAL OF SOLIDS and STRUCTURES

www.elsevier.com/locate/ijsolstr

# An efficient approach for the numerical inversion of Laplace transform and its application in dynamic fracture analysis of a piezoelectric laminate

Xiaohua Zhao *

*Department of Civil Engineering, Shantou University, Shantou 515063, China*

Received 22 December 2002; received in revised form 7 December 2003
Available online 11 March 2004

**Abstract**

A numerical method is developed for the inversion of Laplace transform, and its accuracy is shown through examples. As an application of the method, the transient analysis of a piezoelectric laminate with multiple interfacial cracks is performed. Both the permeable and impermeable boundary conditions are discussed. The solution procedures are based on the use of integral transforms, singular integral equations and Chebyshev polynomial expansions. Numerical results are provided to show the effect of crack geometry, applied electric fields, electric boundary conditions along the crack faces and the wave fronts of incident waves or the reflecting waves from surface boundaries on the resulting dynamic stress intensity factor and electric displacement intensity factor.


*Keywords:* Inversion; Laplace transform; Transient; Piezoelectric laminate; Crack

## 1. Introduction

With the increasing usage of piezoelectric materials and composites as actuating and sensing devices in advanced structural design to form a self-controlling and self-monitoring smart system, much attention has been paid to the study of their dynamic fracture behavior in recent years. A comprehensive body of knowledge exists addressing the responses of cracked piezoelectric materials and composites subjected to *steady state* loading, and efforts have been made to achieve an in depth understanding of the electro-elastic failure mechanism of the materials and composites with one single crack (see, e.g., Narita and Shindo, 1998, 1999), or with multiple cracks (see, e.g., Meguid and Wang, 1998; Wang and Meguid, 2000; Wang, 2001) as well as with debonding (see, e.g., Zhao and Meguid, 2002).

* Tel.: +86-75-4290-2553; fax: +86-75-4290-2005.
*E-mail address:* xhzhao@stu.edu.cn (X. Zhao).

0020-7683/$ - see front matter © 2004 Elsevier Ltd. All rights reserved.
doi:10.1016/j.ijsolstr.2004.01.006

In engineering applications, piezoelectric materials and composites are often subjected to *transient loading*, such as impact, explosion, and transient electric fields. However, very few works are concerned with the *transient response* of cracked piezoelectric materials and composites. Among the limited studies, Li and Mataga (1996a,b) investigated the problem of a semi-infinite crack propagating in an infinite piezoelectric medium. They studied the effect of the propagating velocity of the crack on the crack tip fields. Chen and Yu (1997), Chen and Karihaloo (1999) investigated the transient response of a finite crack in an infinite piezoelectric medium under the action of anti-plane mechanical loads and in-plane electric displacements. Meguid and Chen (2001), Wang and Yu (2000), and Shin et al. (2001) considered the dynamic crack problem in a piezoelectric strip under electro-mechanical impact. Wang et al. (2000) analyzed a cracked piezoelectric laminate subjected to electro-mechanical impact loads. In their recent work, Meguid and Zhao (2002) studied the interface crack problem of bonded piezoelectric and elastic half space under transient electro-mechanical loads.

From the analyses concerning the transient response of cracked piezoelectric materials and composites, it can be seen that Laplace transform is usually utilized to suppress the dependence on time. In the transform domain, the boundary value problems may be reduced to dual integral equations or a set of coupled singular integral equations, which are solved by using the Copson–Sih's method or Chebyshev polynomial expansions. To invert the solutions to the physical plane, the inversion of Laplace transform must be made.

Presently, over twenty methods have been developed for the inversion. Among them both the Miller/Guy's method and the Durbin's method were widely used in the field of dynamic fracture mechanics (see, e.g., Chen and Yu, 1997; Chen and Karihaloo, 1999; Meguid and Chen, 2001; Wang and Yu, 2000; Shin et al., 2001; Wen et al., 1996a,b). Narayanan and Beskos (1982) made a comparison study of these methods and found that the best one of them is the Durbin's method (Durbin, 1974). Though the Miller/Guy's method has been used in most of the existing studies concerning the dynamic fracture of piezoelectric materials due to its simplicity, it is shown that this method cannot achieve good results and its accuracy is usually poor in numerical calculation.

In the author's practice, both the Miller/Guy's method and the Durbin's method were used to investigate the dynamic crack problems of piezoelectric materials. It was found that the Miller/Guy's method gave diverging and inaccurate results when a finite geometry was present (Meguid and Zhao, 2002). In fact, the Miller/Guy's method is based on the expansion of orthogonal polynomials which are smooth, and therefore cannot describe correctly the interaction between cracks and the wave fronts of incident waves or the reflecting waves from surface boundaries with only a few of expansion terms. Theoretically, this drawback may be overcome by increasing the number of the terms. But, when the number exceeds 11, the coefficients of the expansion become so small that a numerical instability happens. Moreover, this method strongly depends on the choice of two parameters, and different choices may lead to quite different solutions.

As Naraynan and Beskos tested, the Durbin's method can give reliable results in most cases. However, this method still suffers from one drawback for long time inversion. Namely, the inversion may become highly oscillatory or get away from the right solution with the increase of time in some cases.

In the present paper, an accurate method is developed for the inversion, which overcomes the drawback of the Durbin's method. Numerical results show that the proposed method can achieve more reliable inversion than the Durbin's method for long time inversion.

As an application of the method, the transient analysis of a piezoelectric laminate with multiple interfacial cracks is performed. Both the permeable and impermeable boundary conditions are discussed. The solution procedures are based on the use of integral transforms, singular integral equations and Chebyshev polynomial expansions. Numerical results are provided to show the effect of crack geometry, applied electric fields, the electric boundary conditions along the crack faces, incident waves and the reflecting waves from surface boundaries on the resulting dynamic stress intensity factor and electric displacement intensity factor.

## 2. Numerical inversion of Laplace transform

### 2.1. Method

Suppose that $f(t)$ is a real function of $t$, with $f(t) = 0$ for $t < 0$. The Laplace transform of the function and its inversion are defined as follows:

$$f^*(p) = \int_0^\infty f(t)\exp(-pt)\,\mathrm{d}t, \tag{1}$$

$$f(t) = \frac{1}{2\pi\mathrm{i}}\int_{\alpha-\mathrm{i}\infty}^{\alpha+\mathrm{i}\infty} f^*(p)\exp(pt)\,\mathrm{d}p, \tag{2}$$

where $p$ is the complex transform parameter and $\alpha$ is a real number greater than the real parts of all singularities of $f^*(p)$.

When $f^*(p)$ becomes known, the inversion may be obtained with the theory of complex analysis. However, in the field of dynamic fracture analysis, $f^*(p)$ is usually given at discrete points, and therefore the integral in (2) cannot be analytically evaluated. As an alternative, numerical inversion is used.

Let $p = \alpha + \mathrm{i}\omega$, then we have (Durbin, 1974)

$$f(0) = \frac{1}{\pi}\int_0^\infty \mathrm{Re}[f^*(\alpha+\mathrm{i}\omega)]\,\mathrm{d}\omega \quad \text{for } t = 0, \tag{3a}$$

$$f(t) = \frac{\exp(\alpha t)}{\pi}\int_0^\infty \{\mathrm{Re}[f^*(\alpha+\mathrm{i}\omega)]\cos\omega t - \mathrm{Im}[f^*(\alpha+\mathrm{i}\omega)]\sin\omega t\}\,\mathrm{d}\omega \quad \text{for } t > 0. \tag{3b}$$

Durbin (1974) developed a method to calculate the above integrals numerically, which can be written as

$$f(t) \approx \frac{2\exp(\alpha t)}{T}\left\langle -\frac{1}{2}\mathrm{Re}f^*(\alpha) + \sum_{k=0}^{\infty}\left\{\mathrm{Re}\left[f^*\left(\alpha+\mathrm{i}k\frac{2\pi}{T}\right)\right]\cos k\frac{2\pi}{T}t - \mathrm{Im}\left[f^*\left(\alpha+\mathrm{i}k\frac{2\pi}{T}\right)\right]\sin k\frac{2\pi}{T}t\right\}\right\rangle. \tag{4}$$

Formula (4) is valid over the interval $[0, T]$, and is formally equivalent to the application of the trapezoidal rule to (3a) and (3b), with the integration step being $2\pi/T$. Practically, the infinite series can only be summed up to a number NSUM of terms.

For short time inversion, this method always gives good results. The reason is that a short time solution depends mainly on the large value of the transform parameter $p$ (according to the initial-value theorem), which indicates that a large interval of $\omega$ is needed to calculate the integrals in (3a) and (3b). In this case, since the time length $T$ is short, $2\pi/T$ becomes large, and the summation in formula (4) covers a large interval of $\omega$ (with a fixed NSUM). Therefore, good results can be obtained.

However, the long time inversion with the method may become highly oscillatory or get away from the right solution. As we know from the final-value theorem, a long time inversion depends mainly on the initial value of $p$. That is to say, an accurate estimation of the integrals in (3a) and (3b) should be made over the interval from 0 to a certain value of $\omega$, for example, $\omega = 5.0$. To achieve this, a small integration step is required. But, for a given time length, $2\pi/T$ is usually not small enough so that much error is induced.

This drawback arises from the use of a constant integration step. In fact, we do not need to do so. We know that the transformed function $f^*(p)$ has the property

$$f^*(p) = \mathrm{O}(p^{-m}), \quad |p| \to \infty, \ m > 0, \tag{5}$$

which implies that $|f^*(p)|$ may become small as $|p|$ tends to a certain value, for example, $|p| = 50$. This property allows us to use different integration steps for calculating the integrals in (3a) and (3b) numerically, and thus, good accuracy can be achieved with much less effort. In the next, two algorithms are developed.

**Algorithm 1.** Divide the integration interval into small sub-spaces, and denote the nodes with $\omega_k$ ($k = 1, 2, \ldots, \infty$). Then, the integrals in (3a) and (3b) become

$$f(0) = \frac{1}{\pi}\sum_{k=1}^{\infty}\int_{\omega_k}^{\omega_{k+1}} \mathrm{Re}[f^*(\alpha + \mathrm{i}\omega)]\,\mathrm{d}\omega \quad \text{for } t = 0, \tag{6a}$$

$$f(t) = \frac{\exp(\alpha t)}{\pi}\sum_{k=1}^{\infty}\int_{\omega_k}^{\omega_{k+1}} \{\mathrm{Re}[f^*(\alpha + \mathrm{i}\omega)]\cos\omega t - \mathrm{Im}[f^*(\alpha + \mathrm{i}\omega)]\sin\omega t\}\,\mathrm{d}\omega \quad \text{for } t > 0. \tag{6b}$$

In each sub-space of $[\omega_k, \omega_{k+1}]$, we approximate $\mathrm{Re}[f^*(\alpha + \mathrm{i}\omega)]$ and $\mathrm{Im}[f^*(\alpha + \mathrm{i}\omega)]$ with linear functions respectively, which are expressed as

$$\mathrm{Re}[f^*(\alpha + \mathrm{i}\omega)] \approx F_k + \frac{F_{k+1} - F_k}{\omega_{k+1} - \omega_k}(\omega - \omega_k), \tag{7a}$$

$$\mathrm{Im}[f^*(\alpha + \mathrm{i}\omega)] \approx G_k + \frac{G_{k+1} - G_k}{\omega_{k+1} - \omega_k}(\omega - \omega_k), \tag{7b}$$

where

$$F_k = \mathrm{Re}[f^*(\alpha + \mathrm{i}\omega_k)], \qquad F_{k+1} = \mathrm{Re}[f^*(\alpha + \mathrm{i}\omega_{k+1})], \tag{8}$$

$$G_k = \mathrm{Im}[f^*(\alpha + \mathrm{i}\omega_k)], \qquad G_{k+1} = \mathrm{Im}[f^*(\alpha + \mathrm{i}\omega_{k+1})]. \tag{9}$$

Substituting (7a) and (7b) into (6a) and making a direct integration, we have

$$f(0) \approx \sum_{k=1}^{\infty}\frac{(F_k + F_{k+1})\Delta_k}{2\pi}, \tag{10}$$

where $\Delta_k = \omega_{k+1} - \omega_k$.

The integral in (6b) can be evaluated by

$$\begin{aligned} f(t) \approx \frac{\exp(\alpha t)}{\pi}\sum_{k=1}^{\infty}\Bigg\{ & \frac{F_{k+1}\sin\omega_{k+1}t - F_k\sin\omega_k t}{t} + \frac{F_{k+1} - F_k}{\Delta_k}\frac{\cos\omega_{k+1}t - \cos\omega_k t}{t^2} \\ & + \frac{G_{k+1}\cos\omega_{k+1}t - G_k\cos\omega_k t}{t} - \frac{G_{k+1} - G_k}{\Delta_k}\frac{\sin\omega_{k+1}t - \sin\omega_k t}{t^2}\Bigg\}. \end{aligned} \tag{11}$$

Noting that $\omega_1 = 0$, and both $F_k$ and $G_k$ tend to zero as $k \to \infty$, we finally have

$$f(t) \approx \frac{\exp(\alpha t)}{\pi t^2}\sum_{k=1}^{\infty}\left[\frac{F_{k+1} - F_k}{\Delta_k}(\cos\omega_{k+1}t - \cos\omega_k t) - \frac{G_{k+1} - G_k}{\Delta_k}(\sin\omega_{k+1}t - \sin\omega_k t)\right]. \tag{12}$$

Formula (10) has the same precision as one when the trapezoidal rule is used. The error estimation for (12) may be made as follows:

$$\begin{aligned}
\text{Error} &= \frac{\exp(\alpha t)}{\pi}\sum_{k=1}^{\infty}\int_{\omega_k}^{\omega_{k+1}}\left\{\mathrm{Re}[f^*(\alpha+\mathrm{i}\omega)]-\left[F_k+\frac{F_{k+1}-F_k}{\Delta_k}(\omega-\omega_k)\right]\right\}\cos\omega t\,\mathrm{d}\omega \\
&\quad -\frac{\exp(\alpha t)}{\pi}\sum_{k=1}^{\infty}\int_{\omega_k}^{\omega_{k+1}}\left\{\mathrm{Im}[f^*(\alpha+\mathrm{i}\omega)]-\left[G_k+\frac{G_{k+1}-G_k}{\Delta_k}(\omega-\omega_k)\right]\right\}\sin\omega t\,\mathrm{d}\omega \\
&= \frac{\exp(\alpha t)}{2\pi}\sum_{k=1}^{\infty}\int_{\omega_k}^{\omega_{k+1}}\frac{\mathrm{d}^2}{\mathrm{d}\omega^2}\{\mathrm{Re}f^*[\alpha+\mathrm{i}(\omega_k+\theta_k\Delta_k)]\}(\omega-\omega_k)(\omega-\omega_{k+1})\cos\omega t\,\mathrm{d}\omega \\
&\quad -\frac{\exp(\alpha t)}{2\pi}\sum_{k=1}^{\infty}\int_{\omega_k}^{\omega_{k+1}}\frac{\mathrm{d}^2}{\mathrm{d}\omega^2}\{\mathrm{Im}f^*[\alpha+\mathrm{i}(\omega_k+\theta_{k1}\Delta_k)]\}(\omega-\omega_k)(\omega-\omega_{k+1})\sin\omega t\,\mathrm{d}\omega \\
&= -\frac{\exp(\alpha t)\Delta_k^3}{12\pi}\sum_{k=0}^{\infty}\left\langle\frac{\mathrm{d}^2}{\mathrm{d}\omega^2}\left\{\mathrm{Re}f^*[\alpha+\mathrm{i}(\omega_k+\bar\theta_k\Delta_k)]\right\}\cos(\omega_k+\bar\theta_k\Delta_k)t\right. \\
&\quad \left.-\frac{\mathrm{d}^2}{\mathrm{d}\omega^2}\left\{\mathrm{Im}f^*[\alpha+\mathrm{i}(\omega_k+\bar\theta_{k1}\Delta_k)]\right\}\sin(\omega_k+\bar\theta_{k1}\Delta_k)t\right\rangle, \qquad (13)
\end{aligned}$$

where $0<\theta_k,\bar\theta_k,\theta_{k1},\bar\theta_{k1}<1$.

**Algorithm 2.** Supposing that $R$ is a large real number, we have

$$f(0)=\frac{1}{\pi}\lim_{R\to\infty}\int_0^R\mathrm{Re}[f^*(\alpha+\mathrm{i}\omega)]\,\mathrm{d}\omega\quad\text{for } t=0, \qquad (14a)$$

$$f(t)=\frac{\exp(\alpha t)}{\pi}\lim_{R\to\infty}\int_0^R\{\mathrm{Re}[f^*(\alpha+\mathrm{i}\omega)]\cos\omega t-\mathrm{Im}[f^*(\alpha+\mathrm{i}\omega)]\sin\omega t\}\,\mathrm{d}\omega\quad\text{for } t>0. \qquad (14b)$$

Divide $[0,R]$ into $n$ small sub-spaces, and the nodes are given by $0=\omega_1<\omega_2<\cdots<\omega_n<\omega_{n+1}=R$. Then, (14a) and (14b) can be expressed approximately as

$$f(0)\approx\frac{1}{\pi}\sum_{k=1}^{n}\int_{\omega_k}^{\omega_{k+1}}\mathrm{Re}[f^*(\alpha+\mathrm{i}\omega)]\,\mathrm{d}\omega\quad\text{for } t=0, \qquad (15a)$$

$$f(t)\approx\frac{\exp(\alpha t)}{\pi}\sum_{k=1}^{n}\int_{\omega_k}^{\omega_{k+1}}\{\mathrm{Re}[f^*(\alpha+\mathrm{i}\omega)]\cos\omega t-\mathrm{Im}[f^*(\alpha+\mathrm{i}\omega)]\sin\omega t\}\,\mathrm{d}\omega\quad\text{for } t>0. \qquad (15b)$$

In each sub-space of $[\omega_k,\omega_{k+1}]$ $(k=1,2,\ldots,n)$, The functions $\mathrm{Re}[f^*(\alpha+\mathrm{i}\omega)]$ and $\mathrm{Im}[f^*(\alpha+\mathrm{i}\omega)]$ are approximated with Subbotin-splines respectively, that is (Cheney and Kincaid, 1985)

$$\mathrm{Re}[f^*(\alpha+\mathrm{i}\omega)]\approx F_k+\frac{1}{2}(Z_{k+1}+Z_k)(\omega-\tau_k)+\frac{1}{2\Delta_k}(Z_{k+1}-Z_k)(\omega-\tau_k)^2, \qquad (16a)$$

$$\mathrm{Im}[f^*(\alpha+\mathrm{i}\omega)]\approx G_k+\frac{1}{2}(Y_{k+1}+Y_k)(\omega-\tau_k)+\frac{1}{2\Delta_k}(Y_{k+1}-Y_k)(\omega-\tau_k)^2, \qquad (16b)$$

where

$$\Delta_k=\omega_{k+1}-\omega_k, \qquad (17a)$$

$$\tau_k=\frac{1}{2}(\omega_{k+1}+\omega_k), \qquad (17b)$$

$$F_k = \mathrm{Re}[f^*(\alpha + \mathrm{i}\tau_k)], \tag{17c}$$

$$G_k = \mathrm{Im}[f^*(\alpha + \mathrm{i}\tau_k)]. \tag{17d}$$

$Z_k$ $(k = 1, 2, \ldots, n+1)$ are determined by the following equations:

$$3\Delta_1 Z_1 + \Delta_1 Z_2 = 8(F_1 - F_0), \tag{18a}$$

$$\Delta_{k-1} Z_{k-1} + 3(\Delta_k + \Delta_{k-1}) Z_k + \Delta_k Z_{k+1} = 8(F_k - F_{k-1}) \quad (k = 2, 3, \ldots, n), \tag{18b}$$

$$3\Delta_n Z_{n+1} + \Delta_n Z_n = 8(F_{n+1} - F_n), \tag{18c}$$

where $F_0 = \mathrm{Re}[f^*(\alpha + \mathrm{i}\omega_1)]$ and $F_{n+1} = \mathrm{Re}[f^*(\alpha + \mathrm{i}\omega_{n+1})]$.

$Y_k$ $(k = 1, 2, \ldots, n+1)$ are determined by

$$3\Delta_1 Y_1 + \Delta_1 Y_2 = 8(G_1 - G_0), \tag{19a}$$

$$\Delta_{k-1} Y_{k-1} + 3(\Delta_k + \Delta_{k-1}) Y_k + \Delta_k Y_{k+1} = 8(G_k - G_{k-1}) \quad (k = 2, 3, \ldots, n), \tag{19b}$$

$$3\Delta_n Y_{n+1} + \Delta_n Y_n = 8(G_{n+1} - G_n), \tag{19c}$$

where $G_0 = \mathrm{Im}[f^*(\alpha + \mathrm{i}\omega_1)]$ and $G_{n+1} = \mathrm{Im}[f^*(\alpha + \mathrm{i}\omega_{n+1})]$.

Using the expressions (16a) and (16b) and making a direct integration to (15a) and (15b), we have

$$f(0) \approx \frac{1}{\pi} \sum_{k=1}^{n} \left[ F_k + \frac{\Delta_k}{24} (Z_{k+1} - Z_k) \right] \Delta_k, \tag{20a}$$

$$f(t) \approx \frac{\exp(\alpha t)}{\pi} \left\{ \frac{1}{t} g_1(t) + \frac{1}{t^2} g_2(t) - \sum_{k=1}^{n} \frac{1}{t^3 \Delta_k} [(Z_{k+1} - Z_k)(\sin \omega_{k+1} t - \sin \omega_k t) + (Y_{k+1} - Y_k)(\cos \omega_{k+1} t - \cos \omega_k t)] \right\}, \tag{20b}$$

where

$$g_1(t) = \left[ F_n + \frac{1}{8} (Z_n + 3Z_{n+1}) \Delta_n \right] \sin \omega_{n+1} t + \frac{1}{8} (Y_2 + 3Y_1) \Delta_1 - G_1 + \left[ G_n + \frac{1}{8} (Y_n + 3Y_{n+1}) \Delta_n \right] \cos \omega_{n+1} t, \tag{21a}$$

$$g_2(t) = -Z_1 + Z_{n+1} \cos \omega_{n+1} t - Y_{n+1} \sin \omega_{n+1} t. \tag{21b}$$

Truncation error and interpolation error will be induced when using (20a) and (20b) for inversion. The truncation error may be reduced as long as $R$ is large enough. From the theory of spline functions, the interpolation error due to (16a) or (16b) is of the order $\mathrm{O}(\Delta_{\max}^3)$ (Li and Qi, 1979), with $\Delta_{\max} = \max |\omega_{k+1} - \omega_k|$. Therefore, the error induced by (20a) or (20b) is of the order $\mathrm{O}(\Delta_{\max}^4)$.

### 2.2. Examples

From formulas (10), (12), (20a) and (20b), it is seen that the lengths of all sub-spaces can be different, which allows us to achieve good accuracy with less effort. Moreover, these formulas are derived from the definition of an integral. Therefore, the summations in the formulas are always convergent when $\Delta_{\max} \to 0$ and $n \to \infty$.

For practical applications, both $\Delta_{\max}$ and $n$ are finite, and thus truncation error and interpolation error are induced. Further, the errors are amplified by the factor $\exp(\alpha t)/\pi$ in (12) and (20b), which means that the errors tend to be infinite with the increase of time. To overcome this drawback, we fix $\alpha T$ to a definite value, with $T$ being the time length of inversion. In this way, the errors can always be kept in a reasonable range when $t < T$. Then, the parameter $\alpha$ is determined. According to the definition of Laplace transform and its inversion, $\alpha$ is a real number greater than the real parts of all singularities of $f^*(p)$. We have tried many cases and found that good results can be obtained if it is taken as

$$\alpha = \max[\mathrm{Re}(p_i)] + \frac{5}{T},$$

where $p_i$ $(i = 1, 2, \ldots)$ express all singular points of $f^*(p)$. The same $\alpha$ is also used in the Durbin's method.

Three examples are given here:

**Example 1.** $f^*(p) = p^{-1}$, $f(t) = H(t)$.

**Example 2.** $f^*(p) = p(p^2 + 1)^{-2}$, $f(t) = (t/2)\sin(t)$.

**Example 3.** $f^*(p) = (p - 3)^{-1}$, $f(t) = \exp(3t)$.

The time lengths are chosen to be $T = 20$ for Examples 1 and 2, and $T = 4$ for Example 3. In the computation, the whole range of integration is divided into three intervals: $[0, 2.5]$, $[2.5, 37.5]$ and $[37.5, 897.5]$. A constant step $\Delta_k = 0.005$ is used for all sub-spaces in $[0, 2.5]$, while $\Delta_k = 0.5$ and $\Delta_k = 2.0$ are taken for sub-spaces in $[2.5, 37.5]$ and $[37.5, 897.5]$, respectively. The total number of summations is 1000 terms.

Results are shown in Tables 1–3. It is shown that the present solutions agree well with exact ones. However, the inversions of Examples 1 and 3 by using the Durbin's method get away with the increase of time.

Finally, it should be pointed out that the choice of integration steps has a great effect on the inversion. Theoretically, smaller the integration steps are, more accurate the inversion will be. However, much computation effort will be required, which is time consuming in the field of dynamic fracture mechanics. For reference, we recommend the use of Table 4. To our practice, good accuracy can be obtained for $t \leqslant T$ with values in this Table. To achieve better results, smaller integration steps are needed.

## 3. Application in dynamic fracture analysis of a piezoelectric laminate

### 3.1. Problem statement

Consider the problem of a piezoelectric laminate containing $n$ interfacial collinear cracks, as shown in Fig. 1. A set of Cartesian coordinates $(x, y, z)$ is chosen such that the $x$-axis is directed along the crack line and $y$-axis is perpendicular to it. The poled piezoelectric strip, with the $z$-axis being the poling direction, occupies the region $(-h < y < 0, -\infty < x < +\infty)$.

In a previous paper (Zhao and Meguid, 2002), the author(s) discussed the dynamic behavior of the laminate under steady-state electro-mechanical loading, and the dependency of both the local stress and electrical fields at crack tips on frequencies of loading was examined. Here, the transient behavior of the laminate is studied. Suppose that the laminate is initially stress free and at rest. At time $t = 0$, a pair of uniform shear stresses of $\tau_0 H(t)$ suddenly appear on the surfaces of $y = -h$ and $h_1$ $(-\infty < x < +\infty)$, respectively. A uniform in-plane electric displacement $D_0 H(t)$ is also applied on the lower surface of the

Table 1
Inversion of the function $f^*(p) = p^{-1}$

| $t$ | Algorithm 1 | Algorithm 2 | Durbin's method | Exact |
|---|---|---|---|---|
| 0.00 | 0.50002454 | 0.49998200 | 0.50653049 | 1.00000000 |
| 1.00 | 0.99984388 | 0.99999402 | 1.00549358 | 1.00000000 |
| 2.00 | 0.99995698 | 1.00000370 | 1.00597629 | 1.00000000 |
| 3.00 | 1.00016226 | 1.00002421 | 1.00612267 | 1.00000000 |
| 4.00 | 0.99973049 | 1.00001323 | 1.00618855 | 1.00000000 |
| 5.00 | 1.00017907 | 0.99999158 | 1.00622859 | 1.00000000 |
| 6.00 | 0.99975946 | 0.99998448 | 1.00626599 | 1.00000000 |
| 7.00 | 0.99995896 | 0.99996924 | 1.00631770 | 1.00000000 |
| 8.00 | 0.99992645 | 1.00001701 | 1.00640245 | 1.00000000 |
| 9.00 | 0.99966112 | 1.00001107 | 1.00654564 | 1.00000000 |
| 10.00 | 1.00004361 | 1.00003587 | 1.00678511 | 1.00000000 |
| 11.00 | 0.99944320 | 0.99999743 | 1.00717982 | 1.00000000 |
| 12.00 | 1.00009414 | 0.99997066 | 1.00782468 | 1.00000000 |
| 13.00 | 0.99923983 | 0.99996375 | 1.00887807 | 1.00000000 |
| 14.00 | 0.99977563 | 0.99999187 | 1.01061669 | 1.00000000 |
| 15.00 | 0.99945386 | 1.00003359 | 1.01355593 | 1.00000000 |
| 16.00 | 0.99948358 | 1.00002965 | 1.01874996 | 1.00000000 |
| 17.00 | 0.99940670 | 1.00002235 | 1.02868949 | 1.00000000 |
| 18.00 | 0.99931966 | 0.99996898 | 1.05088628 | 1.00000000 |
| 19.00 | 0.99923481 | 0.99995546 | 1.12293998 | 1.00000000 |
| 20.00 | 0.99920029 | 0.99997784 | 75.17073028 | 1.00000000 |

Table 2
Inversion of the function $f^*(p) = p(p^2 + 1)^{-2}$

| $t$ | Algorithm 1 | Algorithm 2 | Durbin's method | Exact |
|---|---|---|---|---|
| 0.00 | −0.00009131 | 0.00000218 | 0.06218747 | 0.00000000 |
| 1.00 | 0.42073715 | 0.42072545 | 0.47977090 | 0.42073549 |
| 2.00 | 0.90949537 | 0.90931095 | 0.90776061 | 0.90929743 |
| 3.00 | 0.21129895 | 0.21166887 | 0.14529924 | 0.21168001 |
| 4.00 | −1.51309243 | −1.51360309 | −1.58679915 | −1.51360499 |
| 5.00 | −2.39762968 | −2.39729723 | −2.40758056 | −2.39731069 |
| 6.00 | −0.83785428 | −0.83827882 | −0.77051018 | −0.83824649 |
| 7.00 | 2.29907174 | 2.29950339 | 2.38657029 | 2.29945310 |
| 8.00 | 3.95684237 | 3.95736997 | 3.98214155 | 3.95743299 |
| 9.00 | 1.85447616 | 1.85460021 | 1.78863406 | 1.85453318 |
| 10.00 | −2.71993636 | −2.72016580 | −2.82025465 | −2.72010555 |
| 11.00 | −5.49808585 | −5.49990224 | −5.54135701 | −5.49994614 |
| 12.00 | −3.21897264 | −3.21946065 | −3.15882255 | −3.21943751 |
| 13.00 | 2.73054498 | 2.73109266 | 2.84272087 | 2.73108574 |
| 14.00 | 6.93118737 | 6.93426442 | 6.99415956 | 6.93425149 |
| 15.00 | 4.87496126 | 4.87712892 | 4.82541788 | 4.87715880 |
| 16.00 | −2.30199547 | −2.30319122 | −2.42416899 | −2.30322653 |
| 17.00 | −8.16699679 | −8.17190744 | −8.25152215 | −8.17187868 |
| 18.00 | −6.75430215 | −6.75886561 | −6.71963241 | −6.75888522 |
| 19.00 | 1.42278407 | 1.42382934 | 1.55131243 | 1.42383349 |
| 20.00 | 9.12178084 | 9.12944158 | 9.22943796 | 9.12945251 |

piezoelectric strip at $y = -h$ and $-\infty < x < +\infty$. Further, it is assumed that the surface of the elastic material is grounded.

Table 3
Inversion of the function $f^*(p) = (p-3)^{-1}$

| $t$ | Algorithm 1 | Algorithm 2 | Durbin's method | Exact |
|---|---|---|---|---|
| 0.00 | 0.50011 | 0.49990 | 0.51845 | 1.00000 |
| 0.20 | 1.82371 | 1.82227 | 1.85388 | 1.82212 |
| 0.40 | 3.32303 | 3.31988 | 3.37964 | 3.32012 |
| 0.60 | 6.05297 | 6.04981 | 6.15908 | 6.04965 |
| 0.80 | 11.02414 | 11.02337 | 11.22347 | 11.02318 |
| 1.00 | 20.07887 | 20.08441 | 20.45160 | 20.08554 |
| 1.20 | 36.57620 | 36.60217 | 37.26702 | 36.59823 |
| 1.40 | 66.64184 | 66.67833 | 67.90862 | 66.68633 |
| 1.60 | 121.44564 | 121.52586 | 123.74642 | 121.51042 |
| 1.80 | 221.34950 | 221.38227 | 225.50364 | 221.40642 |
| 2.00 | 403.45759 | 403.44949 | 410.95599 | 403.42879 |
| 2.20 | 735.35683 | 735.08906 | 748.97798 | 735.09519 |
| 2.40 | 1340.13471 | 1339.32859 | 1365.18590 | 1339.43076 |
| 2.60 | 2441.93443 | 2440.91071 | 2488.80487 | 2440.60198 |
| 2.80 | 4448.95332 | 4446.31800 | 4538.50014 | 4447.06675 |
| 3.00 | 8104.69090 | 8104.66910 | 8280.18378 | 8103.08393 |
| 3.20 | 14,762.71065 | 14,762.56279 | 15,119.63179 | 14,764.78157 |
| 3.40 | 26,892.87570 | 26,906.51289 | 27,656.99986 | 26,903.18607 |
| 3.60 | 48,993.56258 | 49,019.90264 | 50,814.33716 | 49,020.80114 |
| 3.80 | 89,268.45788 | 89,315.76271 | 95,000.68321 | 89,321.72336 |
| 4.00 | 162,675.32300 | 162,779.5352 | 4,606,743.89267 | 162,754.79142 |

Table 4
Choice of integration steps

| | $\omega \in [0,5]$ | $\omega \in [5,50]$ | $\omega > 50$ |
|---|---|---|---|
| $T \leqslant 2.0$ | $\Delta_k \leqslant \frac{\pi}{5T}$ | $\Delta_k \leqslant \frac{2\pi}{T}$ | $\Delta_k = (1-2)\frac{2\pi}{T}$ |
| $T > 2.0$ | $\Delta_k \leqslant \frac{\pi}{5T}$ | $\Delta_k \leqslant \frac{2\pi}{T}$ | $\Delta_k = (2-10)\frac{2\pi}{T}$ |

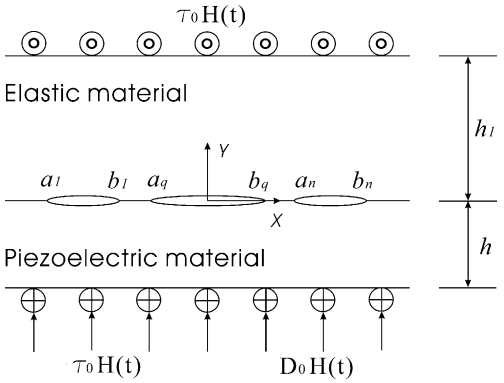


Fig. 1. Geometric configuration of the problem.

Because only the out-of-plane displacement and the in-plane electric fields are nonzero, the constitutive relation for the piezoelectric material can be expressed as

$$\tau_{xz} = c_{44}\frac{\partial w}{\partial x} + e_{15}\frac{\partial \phi}{\partial x}, \qquad \tau_{yz} = c_{44}\frac{\partial w}{\partial y} + e_{15}\frac{\partial \phi}{\partial y}, \tag{22}$$

and

$$D_x = e_{15}\frac{\partial w}{\partial x} - \kappa_{11}\frac{\partial \phi}{\partial x}, \qquad D_y = e_{15}\frac{\partial w}{\partial y} - \kappa_{11}\frac{\partial \phi}{\partial y}, \tag{23}$$

where $\tau_{xz}$ and $\tau_{yz}$ are the shear stress components, $D_x$ and $D_y$ are the electric displacements, $w$ and $\phi$ are the mechanical displacement and electric potential, while $c_{44}$, $e_{15}$ and $\kappa_{11}$ are the elastic modulus, the piezoelectric constant and the dielectric constant of the piezoelectric material, respectively.

The governing equations are given by:

$$\nabla^2 w = c_2^{-2}\frac{\partial^2 w}{\partial^2 t}, \qquad \kappa_{11}\nabla^2\phi = e_{15}\nabla^2 w, \tag{24}$$

where $c_2 = \sqrt{\mu/\rho}$, with $\rho$ being the density of the piezoelectric material and $\mu = c_{44} + e_{15}^2/\kappa_{11}$.

The constitutive relation for the elastic material can be written as

$$\tau_{xz1} = c_{441}\frac{\partial w_1}{\partial x}, \qquad \tau_{yz1} = c_{441}\frac{\partial w_1}{\partial y}, \tag{25}$$

where $\tau_{xz1}$ and $\tau_{yz1}$ are the shear stress components, $w_1$ and $c_{441}$ are the displacement and the elastic modulus, respectively. The governing equation is

$$\nabla^2 w_1 = c_{21}^{-2}\frac{\partial^2 w_1}{\partial t^2}, \tag{26}$$

in which $c_{21} = \sqrt{c_{441}}/\rho_1$ and $\rho_1 =$ the density of the elastic material.

This problem can be treated as the superposition of two sub-problems. Sub-problem (a) considers a crack-free piezoelectric laminate under the action of $\tau_0 H(t)$ and $D_0 H(t)$ at $y = -h$ $(-\infty < x < +\infty)$, and the action of $\tau_0 H(t)$ at $y = h_1$ $(-\infty < x < +\infty)$. While sub-problem (b) concerns a piezoelectric laminate containing multiple interfacial cracks, with the crack faces subjected to the electro-mechanical loads that cancel out the stress and the electric displacement induced by sub-problem (a).

Laplace transform over time $t$ is used to solve those two sub-problems. The solution of sub-problem (a) can be easily obtained and therefore the detailed calculation is omitted. In the transform domain, the stress and the electric displacement along the interface are found to be

$$\overline{\tau}_{yz}^{*}(x,0,p) = \frac{2\tau_0 g_3(p) - e_{15}D_0 g_4(p)/k_{11}}{p g_5(p)}, \tag{27}$$

$$\overline{D}_y^{*}(x,0,p) = D_0/p, \tag{28}$$

where

$$g_3(p) = \exp(ph/c_2)[1 - \exp(2ph_1/c_{21})] + \frac{c_{21}\mu}{c_2 c_{441}}\exp(ph_1/c_{21})[1 - \exp(2ph/c_2)], \tag{29}$$

$$g_4(p) = [1 - \exp(2ph_1/c_{21})][1 - \exp(ph/c_2)]^2, \tag{30}$$

$$g_5(p) = [1 - \exp(2ph_1/c_{21})][1 + \exp(2ph/c_2)] + \frac{c_{21}\mu}{c_2 c_{441}}[1 - \exp(2ph/c_2)][1 + \exp(2ph_1/c_{21})]. \tag{31}$$

The solution of sub-problem (b) can be derived with the help of Fourier transform over the space variable $x$. The governing equations (24) and (26) yield

$$w^*(x,y,p) = \frac{1}{2\pi}\int_{-\infty}^{\infty}[A_1(\xi,p)\exp(-\gamma y) + A_2(\xi,p)\exp(\gamma y)]\exp(-\mathrm{i}\xi x)\,\mathrm{d}\xi, \tag{32}$$

$$\phi^*(x,y,p) = \frac{e_{15}}{\kappa_{11}}w^*(x,y,p) + \psi^*(x,y,p), \tag{33}$$

$$\psi^*(x,y,p) = \frac{1}{2\pi}\int_{-\infty}^{\infty}[A_3(\xi,p)\exp(-|\xi|y) + A_4(\xi,p)\exp(|\xi|y)]\exp(-\mathrm{i}\xi x)\,\mathrm{d}\xi, \tag{34}$$

$$w_1^*(x,y,p) = \frac{1}{2\pi}\int_{-\infty}^{\infty}[A_5(\xi,p)\exp(-\gamma_1 y) + A_6(\xi,p)\exp(\gamma_1 y)]\exp(-\mathrm{i}\xi x)\,\mathrm{d}\xi, \tag{35}$$

where $\gamma = \sqrt{\xi^2 + p^2 c_2^{-2}}$, $\gamma_1 = \sqrt{\xi^2 + p^2 c_{21}^{-2}}$, and $A_j(\xi,p)$ $(j = 1,\ldots,6)$ are unknown functions.

By substituting the above expressions (32)–(35) into the constitutive relations, both the stresses and electric displacements can be obtained.

To determine $A_j(\xi,p)$, we now consider the boundary conditions. For piezoelectric materials, the permeable and impermeable boundary conditions are usually used to model the electric boundary conditions along the crack faces. From the physical viewpoint, these two boundary conditions represent two extreme cases, with the permeable boundary condition being the case that the crack is completely conductive and the impermeable boundary condition being the case that the crack is completely not conductive. Presently, those two boundary conditions are examined and the corresponding discussions are presented in Sections 3.2 and 3.3, respectively.

### 3.2. Solution of the permeable crack problem

In this section, we consider the permeable crack problem. The boundary conditions in Laplace transform domain can be written as

$$\tau_{yz1}^*(x,h_1,p) = 0, \quad -\infty < x < \infty, \tag{36a}$$

$$\tau_{yz1}^*(x,0,p) = \tau_{yz}^*(x,0,p), \quad -\infty < x < \infty, \tag{36b}$$

$$\phi^*(x,0,p) = 0, \quad -\infty < x < \infty, \tag{36c}$$

$$\tau_{yz1}^*(x,0,p) = -\bar{\tau}_{yz}^*(x,0,p), \quad x \in (a_q,b_q), \tag{36d}$$

$$w^*(x,0,p) = w_1^*(x,0,p), \quad x \notin (a_q,b_q), \tag{36e}$$

$$\tau_{yz}^*(x,-h,p) = 0, \quad -\infty < x < \infty, \tag{36f}$$

$$D_y^*(x,-h,p) = 0, \quad -\infty < x < \infty, \tag{36g}$$

where $q = 1,2,\ldots,n$.

The solution procedure is similar to the paper of Zhao and Meguid (2002). If we introduce the following dislocation function by defining:

$$\varphi^*(x,p) = \frac{\partial[w_1^*(x,0,p) - w^*(x,0,p)]}{\partial x} = \begin{cases} 0 & x \notin (a_k,b_k) \\ \varphi_k^*(x,p) & x \in (a_k,b_k) \end{cases} \quad (k = 1,2,\ldots,n). \tag{37}$$

$A_j(\xi,p)$ $(j = 1,\ldots,6)$ can be solved from the above boundary conditions and expressed with $\varphi_k^*(x,p)$.

Define that

$$x = \frac{b_q - a_q}{2}u + \frac{b_q + a_q}{2} = e_q u + d_q, \tag{38}$$

then $\varphi_k^*(x,p)$ $(k = 1,2,\ldots,n)$ must satisfy the following integral equation:

$$\int_{-1}^{1} \frac{\varphi_q^*(\eta,p)}{\eta - u}\,\mathrm{d}\eta + \sum_{k=1}^{n}\int_{-1}^{1} Q_{qk}(\eta,u,p)\varphi_k^*(\eta,p)\,\mathrm{d}\eta = -\frac{\pi(c_{44}+c_{441})}{c_{44}c_{441}}\bar{\tau}_{yz}^*(u,0,p), \quad |u| < 1 \ \ (q = 1,2,\ldots,n), \tag{39}$$

and the single value condition

$$\int_{-1}^{1} \varphi_q^*(\eta,p)\,\mathrm{d}\eta = 0 \quad (q = 1,2,\ldots,n), \tag{40}$$

where

$$\begin{aligned} Q_{qk}(\eta,u,p) = {} & \frac{e_k}{e_k\eta - e_q u + (d_k - d_q)} - \frac{\delta_{qk}}{\eta - u} \\ & - \int_0^\infty e_k\left[\frac{(c_{44}+c_{441})\gamma_1 F_2(\xi,p)}{c_{44}\xi F_1(\xi,p)} + 1\right]\sin[\xi(e_k\eta + d_k) - \xi(e_q u + d_q)]\,\mathrm{d}\xi, \end{aligned} \tag{41}$$

$$\begin{aligned} F_1(\xi,p) = {} & \frac{e_{15}^2}{\kappa_{11}}|\xi|[1+\exp(2\gamma h)][1-\exp(2|\xi|h)][1+\exp(2\gamma_1 h_1)] \\ & + [1+\exp(2|\xi|h)]\{\mu\gamma[1+\exp(2\gamma_1 h_1)][\exp(2\gamma h)-1] - c_{441}\gamma_1[1-\exp(2\gamma_1 h_1)][1+\exp(2\gamma h)]\}, \end{aligned} \tag{42}$$

$$F_2(\xi,p) = [1-\exp(2\gamma_1 h_1)]\big\{\mu\gamma[1+\exp(2|\xi|h)][\exp(2\gamma h)-1] + e_{15}^2/\kappa_{11}|\xi|[1-\exp(2|\xi|h)][1+\exp(2\gamma h)]\big\}, \tag{43}$$

$$e_k = \frac{b_k - a_k}{2}, \qquad d_k = \frac{b_k + a_k}{2}. \tag{44}$$

The solution of Eq. (39) can be written as

$$\varphi_k^*(\eta,p) = \sum_{j=0}^{\infty}\frac{B_{kj}(p)}{\sqrt{1-\eta^2}}T_j(\eta), \tag{45}$$

where $T_j(\eta)$ are Chebyshev polynomials of the first kind and $B_{kj}(p)$ are unknown functions of $p$. From the orthogonality conditions of Chebyshev polynomials, the single value condition leads to $B_{k0}(p) = 0$. Truncating the Chebyshev polynomials in Eq. (45) to the $N$th term and assuming that Eq. (39) is satisfied at $N$ collocation points along the crack faces,

$$u_m = \cos\left(\frac{m\pi}{N+1}\right) \quad (m = 1,2,\ldots,N). \tag{46}$$

Eq. (39) is reduced to a linear algebraic system of equations of the following form:

$$\begin{aligned} & \sum_{j=1}^{N} B_{qj}(p)\sin\left(\frac{mj\pi}{N+1}\right)\Big/\sin\left(\frac{m\pi}{N+1}\right) + \sum_{k=1}^{n}\sum_{j=1}^{N} B_{kj}(p)L_{qkj}(u_m,p) \\ & \quad = -\frac{c_{44}+c_{441}}{c_{44}c_{441}}\bar{\tau}_{yz}^*(u_m,0,p) \quad (m = 1,2,\ldots,N \ \text{ and } \ q = 1,2,\ldots,n), \end{aligned} \tag{47}$$

where

$$L_{qkj}(u_m,p)=\int_{-1}^{1}\frac{T_j(\eta)}{\pi\sqrt{1-\eta^2}}Q_{qk}(\eta,u_m,p)\,\mathrm{d}\eta. \tag{48}$$

Once $B_{qj}(p)$ are obtained from (47), $A_j(\xi,p)$ $(j=1,\ldots,6)$ can be determined. Since the electric displacement is continuous across crack faces, only the stress field at crack tips is singular. The dynamic stress intensity factors of crack $q$ can be evaluated using the following expressions:

$$K_{\mathrm{III}}^{R*}=\lim_{x\to b_q^+}\sqrt{2\pi(x-b_q)}\tau_{yz}^*(x,0,p)=-\frac{c_{44}c_{441}}{c_{44}+c_{441}}\sqrt{\frac{\pi(b_q-a_q)}{2}}\sum_{j=1}^{\infty}B_{qj}(p), \tag{49}$$

$$K_{\mathrm{III}}^{L*}=\lim_{x\to a_q^-}\sqrt{2\pi(a_q-x)}\tau_{yz}^*(x,0,p)=\frac{c_{44}c_{441}}{c_{44}+c_{441}}\sqrt{\frac{\pi(b_q-a_q)}{2}}\sum_{j=1}^{\infty}(-1)^jB_{qj}(p). \tag{50}$$

### 3.3. Solution of the impermeable crack problem

Consider now the impermeable crack problem. The boundary conditions for the problem can be expressed as

$$\tau_{yz1}^*(x,h_1,p)=0,\quad -\infty<x<\infty, \tag{51a}$$

$$\tau_{yz1}^*(x,0,p)=\tau_{yz}^*(x,0,p),\quad -\infty<x<\infty, \tag{51b}$$

$$\tau_{yz}^*(x,0,p)=-\bar{\tau}_{yz}^*(x,0,p),\quad x\in(a_q,b_q), \tag{51c}$$

$$w^*(x,0,p)=w_1^*(x,0,p),\quad x\notin(a_q,b_q), \tag{51d}$$

$$D_y^*(x,0,p)=-D_0/p,\quad x\in(a_q,b_q), \tag{51e}$$

$$\phi^*(x,0,p)=0,\quad x\notin(a_q,b_q), \tag{51f}$$

$$\tau_{yz}^*(x,-h,p)=0,\quad -\infty<x<\infty, \tag{51g}$$

$$D_y^*(x,-h,p)=0,\quad -\infty<x<\infty. \tag{51h}$$

Introduce the following functions:

$$\varphi_1^*(x,p)=\frac{\partial}{\partial x}[w_1^*(x,0,p)-w^*(x,0,p)]=\begin{cases}0 & x\notin(a_k,b_k),\\ \varphi_{1k}^*(x,p) & x\in(a_k,b_k),\end{cases} \tag{52}$$

$$\varphi_2^*(x,p)=-\frac{\partial\phi^*(x,0,p)}{\partial x}=\begin{cases}0 & x\notin(a_k,b_k),\\ \varphi_{2k}^*(x,p) & x\in(a_k,b_k).\end{cases} \tag{53}$$

According to Eqs. (51a)–(51h), $A_j(\xi,p)$ $(j=1,\ldots,6)$ can be expressed with $\varphi_{1k}^*(x,p)$ and $\varphi_{2k}^*(x,p)$. The functions $\varphi_{1k}^*(x,p)$ and $\varphi_{2k}^*(x,p)$ must satisfy the following singular integral equations:

$$\int_{-1}^{1}\frac{\varphi_{1q}^{*}(\eta,p)}{\eta-u}\,\mathrm{d}\eta-\frac{e_{15}}{c_{441}}\int_{-1}^{1}\frac{\varphi_{2q}^{*}(\eta,p)}{\eta-u}\,\mathrm{d}\eta+\sum_{k=1}^{n}\int_{-1}^{1}Q_{11qk}(\eta,u,p)\varphi_{1k}^{*}(\eta,p)\,\mathrm{d}\eta$$
$$-\sum_{k=1}^{n}\int_{-1}^{1}Q_{12qk}(\eta,u,p)\varphi_{2k}^{*}(\eta,p)\,\mathrm{d}\eta=-\frac{\pi(c_{44}+c_{441})}{\mu c_{441}}\left[\bar{\tau}_{yz}^{*}(u,0,p)+\frac{e_{15}}{k_{11}}\frac{D_0}{p}\right],\quad |u|<1, \tag{54}$$

$$-\int_{-1}^{1}\frac{\varphi_{1q}^{*}(\eta,p)}{\eta-u}\,\mathrm{d}\eta+\frac{k_{11}(\mu+c_{441})}{e_{15}c_{441}}\int_{-1}^{1}\frac{\varphi_{2q}^{*}(\eta,p)}{\eta-u}\,\mathrm{d}\eta+\sum_{k=1}^{n}\int_{-1}^{1}Q_{21qk}(\eta,u,p)\varphi_{1k}^{*}(\eta,p)\,\mathrm{d}\eta$$
$$+\sum_{k=1}^{n}\int_{-1}^{1}Q_{22qk}(\eta,u,p)\varphi_{2k}^{*}(\eta,p)\,\mathrm{d}\eta=\frac{\pi(c_{44}+c_{441})}{e_{15}c_{441}}\frac{D_0}{p},\quad |u|<1, \tag{55}$$

and the single value conditions:

$$\int_{-1}^{1}\varphi_{1q}^{*}(\eta,p)\,\mathrm{d}\eta=0,\quad \int_{-1}^{1}\varphi_{2q}^{*}(\eta,p)\,\mathrm{d}\eta=0\qquad (q=1,2,\ldots,n), \tag{56}$$

where

$$Q_{11qk}(\eta,u,p)=\frac{e_k}{e_k\eta-e_qu+(d_k-d_q)}-\frac{\delta_{qk}}{\eta-u}$$
$$-\int_0^{\infty}e_k\left[\frac{c_{44}+c_{441}}{c_{441}}a_{11}(\xi,p)+1\right]\sin[\xi(e_k\eta+d_k)-\xi(e_qu+d_q)]\,\mathrm{d}\xi, \tag{57}$$

$$Q_{12qk}(\eta,u,p)=\frac{e_{15}}{c_{441}}\left[\frac{e_k}{e_k\eta-e_qu+(d_k-d_q)}-\frac{\delta_{qk}}{\eta-u}\right]$$
$$+\int_0^{\infty}e_k\left[\frac{c_{44}+c_{441}}{c_{441}}a_{12}(\xi,p)-\frac{e_{15}}{c_{441}}\right]\sin[\xi(e_k\eta+d_k)-\xi(e_qu+d_q)]\,\mathrm{d}\xi, \tag{58}$$

$$Q_{21qk}(\eta,u,p)=-\frac{e_k}{e_k\eta-e_qu+(d_k-d_q)}+\frac{\delta_{qk}}{\eta-u}$$
$$+\int_0^{\infty}e_k\left[\frac{k_{11}(c_{44}+c_{441})}{e_{15}c_{441}}a_{21}(\xi,p)+1\right]\sin[\xi(e_k\eta+d_k)-\xi(e_qu+d_q)]\,\mathrm{d}\xi, \tag{59}$$

$$Q_{22qk}(\eta,u,p)=\frac{k_{11}(\mu+c_{441})}{e_{15}c_{441}}\left[\frac{e_k}{e_k\eta-e_qu+(d_k-d_q)}-\frac{\delta_{qk}}{\eta-u}\right]$$
$$+\int_0^{\infty}e_k\left[\frac{k_{11}(c_{44}+c_{441})}{e_{15}c_{441}}a_{22}(\xi,p)-\frac{k_{11}(\mu+c_{441})}{e_{15}c_{441}}\right]\sin[\xi(e_k\eta+d_k)-\xi(e_qu+d_q)]\,\mathrm{d}\xi. \tag{60}$$

The expressions of $a_{11}(\xi,p)$, $a_{12}(\xi,p)$, $a_{21}(\xi,p)$ and $a_{22}(\xi,p)$ are the same as those of the paper of Zhao and Meguid (2002).

In a similar fashion to Section 3.2, the functions $\varphi_{1k}^{*}(\eta,p)$ and $\varphi_{2k}^{*}(\eta,p)$ are defined in terms of the Chebyshev polynomials:

$$\varphi_{1k}^{*}(\eta,p)=\sum_{j=0}^{\infty}\frac{B_{kj}(p)}{\sqrt{1-\eta^2}}T_j(\eta),\qquad \varphi_{2k}^{*}(\eta,p)=\sum_{j=0}^{\infty}\frac{E_{kj}(p)}{\sqrt{1-\eta^2}}T_j(\eta). \tag{61}$$

From (56), it follows that $B_{k0} = E_{k0} = 0$. $B_{kj}(p)$ and $E_{kj}(p)$ can be determined from the following algebraic equations:

$$\sum_{j=1}^{N}\left[\frac{\sin\left(\frac{mj\pi}{N+1}\right)}{\sin\left(\frac{m\pi}{N+1}\right)}\right]B_{qj}(p) - \frac{e_{15}}{c_{441}}\sum_{j=1}^{N}\left[\frac{\sin\left(\frac{mj\pi}{N+1}\right)}{\sin\left(\frac{m\pi}{N+1}\right)}\right]E_{qj}(p) + \sum_{k=1}^{n}\sum_{j=1}^{N}L_{11qkj}(u_m,p)B_{kj}(p)$$
$$-\sum_{k=1}^{n}\sum_{j=1}^{N}L_{12qkj}(u_m,p)E_{kj}(p) = -\frac{c_{44}+c_{441}}{\mu c_{441}}\left[\bar{\tau}^*_{yz}(u_m,0,p) + \frac{e_{15}}{k_{11}}\frac{D_0}{p}\right], \tag{62}$$

$$-\sum_{j=1}^{N}\left[\frac{\sin\left(\frac{mj\pi}{N+1}\right)}{\sin\left(\frac{m\pi}{N+1}\right)}\right]B_{qj}(p) + \frac{k_{11}(\mu+c_{441})}{e_{15}c_{441}}\sum_{j=1}^{N}\left[\frac{\sin\left(\frac{mj\pi}{N+1}\right)}{\sin\left(\frac{m\pi}{N+1}\right)}\right]E_{qj}(p) + \sum_{k=1}^{n}\sum_{j=1}^{N}L_{21qkj}(u_m,p)B_{kj}(p)$$
$$+\sum_{k=1}^{n}\sum_{j=1}^{N}L_{22qkj}(u_m,p)E_{kj}(p) = \frac{c_{44}+c_{441}}{e_{15}c_{441}}\frac{D_0}{p} \quad (q = 1,2,\ldots,n \text{ and } m = 1,2,\ldots,N), \tag{63}$$

where

$$L_{rsqkj}(u_m,p) = \int_{-1}^{1}\frac{1}{\pi\sqrt{1-\eta^2}}Q_{rsqk}(\eta,u_m,p)T_j(\eta)\,\mathrm{d}\eta \quad (r,s = 1,2). \tag{64}$$

The dynamic stress intensity factors and electric displacement intensity factors of crack $q$ are defined as follows:

$$K^{R*}_{\mathrm{III}} = \lim_{x\to b_q^+}\sqrt{2\pi(x-b_q)}\tau^*_{yz}(x,0,p)$$
$$= \frac{\mu}{c_{44}+c_{441}}\sqrt{\frac{\pi(b_q-a_q)}{2}}\left(-c_{441}\sum_{j=1}^{\infty}B_{qj}(p) + e_{15}\sum_{j=1}^{\infty}E_{qj}(p)\right) - \frac{e_{15}}{\kappa_{11}}K^{R*}_D(p), \tag{65}$$

$$K^{R*}_D(p) = \lim_{x\to b_q^+}\sqrt{2\pi(x-b_q)}D^*_y(x,0,p)$$
$$= \frac{1}{c_{44}+c_{441}}\sqrt{\frac{\pi(b_q-a_q)}{2}}\left[-e_{15}c_{441}\sum_{j=1}^{\infty}B_{qj}(p) + k_{11}(\mu+c_{441})\sum_{j=1}^{\infty}E_{qj}(p)\right], \tag{66}$$

$$K^{L*}_{\mathrm{III}}(p) = \lim_{x\to a_q^-}\sqrt{2\pi(a_q-x)}\tau^*_{yz}(x,0,p)$$
$$= \frac{\mu}{c_{44}+c_{441}}\sqrt{\frac{\pi(b_q-a_q)}{2}}\left[c_{441}\sum_{j=1}^{\infty}(-1)^jB_{qj}(p) - e_{15}\sum_{j=1}^{\infty}(-1)^jE_{qj}(p)\right] - \frac{e_{15}}{\kappa_{11}}K^{L*}_D(p), \tag{67}$$

$$K^{L*}_D(p) = \lim_{x\to a_q^-}\sqrt{2\pi(a_q-x)}D^*_y(x,0,p)$$
$$= \frac{1}{c_{44}+c_{441}}\sqrt{\frac{\pi(b_q-a_q)}{2}}\left[e_{15}c_{441}\sum_{j=1}^{\infty}(-1)^jB_{qj}(p) - k_{11}(\mu+c_{441})\sum_{j=1}^{\infty}(-1)^jE_{qj}(p)\right]. \tag{68}$$

### 3.4. Numerical results and discussion

Numerical calculations have been carried out to show the influence of the pertinent parameters. In the following calculations, the piezoelectric material is assumed to be PZT-4, and the elastic material is aluminium. Their elastic, piezoelectric and dielectric properties are as follows (Narita and Shindo, 1999):

$$c_{44} = 2.56 \times 10^{10}\ \mathrm{N/m^2}, \quad e_{15} = 12.7\ \mathrm{C/m^2}, \quad \kappa_{11} = 64.6 \times 10^{-10}\ \mathrm{C/vm}, \quad \rho = 7500\ \mathrm{kg/m^3};$$
$$c_{441} = 2.65 \times 10^{10}\ \mathrm{N/m^2}, \quad \rho_1 = 2706\ \mathrm{kg/m^3}.$$

The convergence of the expansions in (45) and (61) has been checked by Zhao and Meguid (2002), and it is found that good convergence can be reached when the expansion number exceeds 15 terms. In the present case, 20 terms are used.

#### 3.4.1. Single crack solution

In this section, we restrict our attention to the single crack solution. It is assumed that $a_1 = -a$ and $b_1 = a$. Numerical results are shown in Figs. 2–10. In these Figures, normalized parameters are used with SIF $= K^R_{\mathrm{III}}(t)/(\tau_0\sqrt{\pi a})$, EDIF $= K^R_D(t)/(D_0\sqrt{\pi a})$, $T = c_2 t/h$ and $Dh = e_{15}D_0/(\kappa_{11}\tau_0)$.

Fig. 2 shows the comparison between the solutions obtained by using the Durbin's method and the present method. It is seen that before $T = 12$, two methods give comparable results. When $T > 12$, the solution from the Durbin's method begins to oscillate, while the present solution keeps stable.

The interaction between the crack and the incident waves or reflecting waves is also clearly shown. Before $T = 1$, the incident wave from the lower surface does not arrive and SIF is zero. After the arrival of the incident wave at $T = 1$, the SIF begins to rise with increasing time, and reaches a peak, then decreases until the arrival of the first reflecting wave from the lower surface ($T = 3$). The later period of time from $T = 3$ to $T = 8.1$ sees the action of multiple reflecting waves. With the arrival of the incident wave from the top surface, a rapid increase of the SIF is induced. The SIF reaches a maximum about 2.7 at $T = 9.4$, and an indication is that the laminate may be damaged at this time.

Figs. 3–5 are concerned with the results of the permeable crack problem. Specifically, Fig. 3 presents the influence of the strip height on the stress intensity factor. By reducing $h_1$, the peak of the SIF will appear earlier, which reflects the earlier arrival of the incident wave from the top surface. When $h_1 = 2h$, an oscillatory vibration is observed. Clearly, this is due to the continuous action of multiple reflecting waves.

In Fig. 4, the influence of the applied electric fields on the dynamic SIF history is shown. It is seen that this effect varies with time. In the periods from $T = 1$ to $T = 4$ and from $T = 8$ to $T = 11$, the SIF is induced mainly by the electro-elastic waves from the piezoelectric material, and the action of the electric fields is

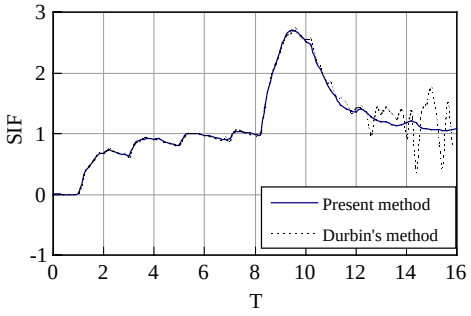


Fig. 2. A comparison between solutions of the Durbin's method and the present method assuming the permeable boundary condition with $h_1 = 10h$, $a/h = 0.5$ and $Dh = 0$.

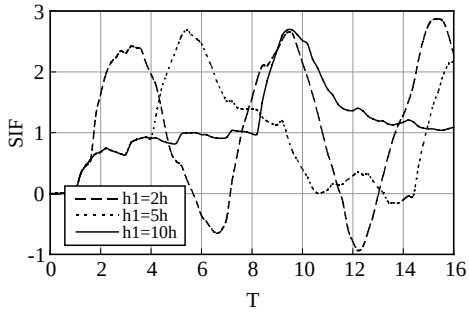


Fig. 3. Normalized SIF versus normalized time for various $h_1$ assuming the permeable boundary condition with $a/h = 0.5$ and $Dh = 0$.

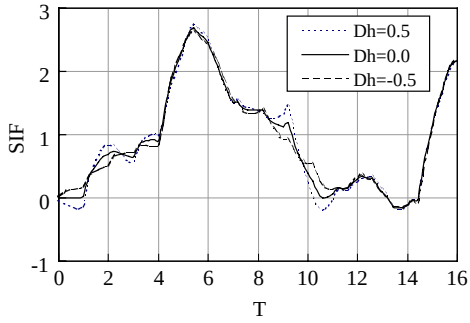


Fig. 4. Normalized SIF versus normalized time for various electro-mechanical loads assuming the permeable boundary condition with $h_1 = 5h$ and $a/h = 0.5$.

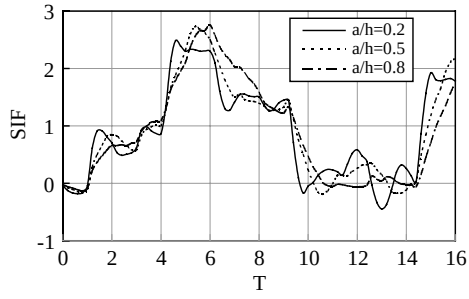


Fig. 5. Normalized SIF versus normalized time for various $a/h$ assuming the permeable boundary condition with $h_1 = 5h$ and $Dh = 0.5$.

obvious, which may lead to the increase or decrease of The SIF. This means that both a positive electric field and a negative electric field can retard or promote the propagation of a crack. The other periods of time see mainly the action of the elastic waves from the upper strip, and as a result the effect of the electric fields is negligible.

Fig. 5 displays the variation of the SIF with various $a/h$ at $Dh = 0.5$.

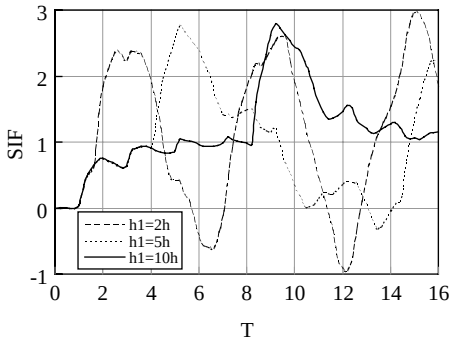


Fig. 6. Normalized SIF versus normalized time for various $h_1$ assuming the impermeable boundary condition with $a/h = 0.5$ and $Dh = 0$.

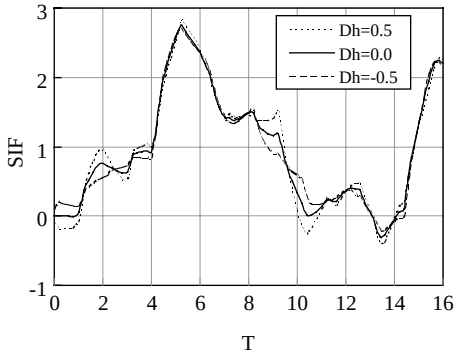


Fig. 7. Normalized SIF versus normalized time for various electro-mechanical loads assuming the impermeable boundary condition with $h_1 = 5h$ and $a/h = 0.5$.

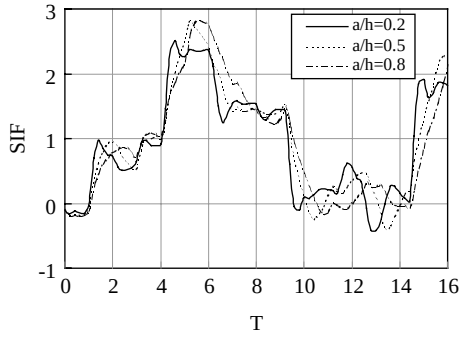


Fig. 8. Normalized SIF versus normalized time for various $a/h$ assuming the impermeable boundary condition with $h_1 = 5h$ and $Dh = 0.5$.

Figs. 6–9 are concerned with the results of the impermeable crack problem. Generally, similar observations may be made from Figs. 6–8. In Fig. 7, one can see that the SIF may be induced by electric fields

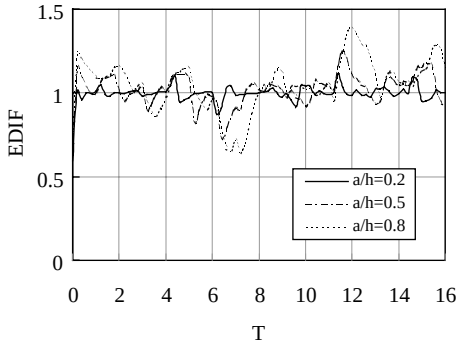


Fig. 9. Normalized EDIF versus normalized time for various $a/h$ assuming the impermeable boundary condition with $h_1 = 5h$ and $Dh = 0.5$.

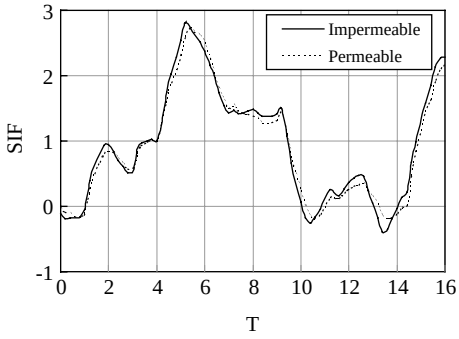


Fig. 10. A comparison between solutions of the permeable and impermeable boundary conditions for $h_1 = 5h$, $a/h = 0.5$ and $Dh = 0.5$.

alone, which is shown before the arrival of the incident electro-elastic waves. It is noticed that at $T = 0$ the SIF has a jump and then keeps almost a constant. From Figs. 6 and 8, one can deduce the influence of the strip height and $a/h$ on the SIF history, respectively.

Fig. 9 displays the time history of the electric displacement intensity factor with various $a/h$ at $Dh = 0.5$. In this Figure, a dynamic overshoot phenomenon is observed. Moreover, the phenomenon is intensified with the increase of $a/h$. This is quite different from the earlier results obtained in Chen and Yu (1997), Chen and Karihaloo (1999), Meguid and Chen (2001), Wang and Yu (2000), and Wang et al. (2000), where the electric displacement intensity factor is in the form of a Heaviside step function.

Finally, a comparison between the solutions of the local stress field for the permeable and impermeable conditions is made in Fig. 10. Obviously, one can see the difference induced by the two electric boundary conditions along the crack faces. However, the difference is not as significant as it is usually thought to be in this case.

*3.4.2. Interacting cracks*

We now present the results of the two-crack solution. It is assumed that $a_1 = -a$, $b_1 = a$, $a_2 = 2a$ and $b_2 = 4a$. The resulting SIF and EDIF at the inner tip of crack one are shown in Figs. 11–13. The corresponding single crack solution is also depicted for comparison.

It is seen from Figs. 11 and 12 that for both the two-crack case and the single crack case, the interaction between a crack and the incident waves or reflecting waves is similar. In the earlier period of time, the SIF

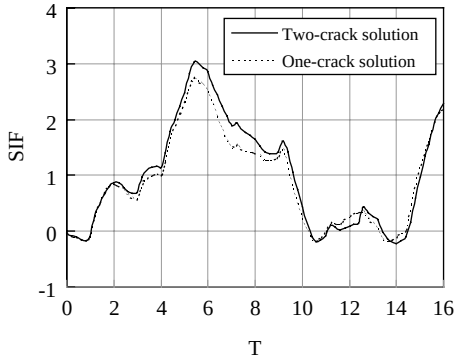


Fig. 11. Normalized SIF versus normalized time assuming the permeable boundary conditions for $h_1 = 5h$, $a/h = 0.5$ and $Dh = 0.5$.

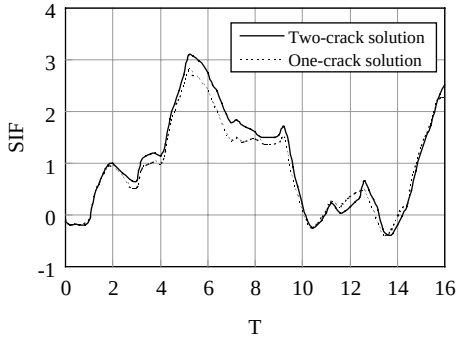


Fig. 12. Normalized SIF versus normalized time assuming the impermeable boundary conditions for $h_1 = 5h$, $a/h = 0.5$ and $Dh = 0.5$.

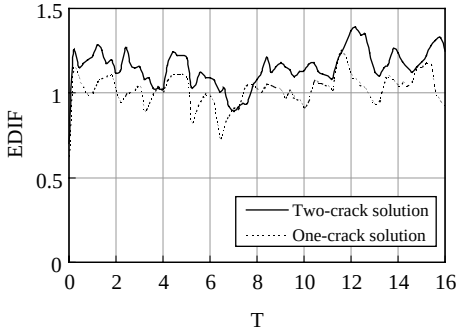


Fig. 13. Normalized EDIF versus normalized time assuming the impermeable boundary conditions for $h_1 = 5h$, $a/h = 0.5$ and $Dh = 0.5$.

solutions are almost the same, which indicates that the influence of crack interaction on the local stress fields of the crack tip is negligible. However, the difference between the two solutions becomes obvious when $T > 2$. The interaction of cracks will lead to the increase of the dynamic stress intensity factor.

Fig. 13 shows the solutions of the electric displacement intensity factor for both the cases. Again, one observes that an overshoot phenomenon occurs, and is intensified due to the interaction of cracks.

## 4. Conclusions

A numerical method is developed for the inversion of the Laplace transform, and its accuracy is demonstrated through examples. As an application of the method, the transient analysis of a piezoelectric laminate with multiple interfacial cracks is performed. The solution procedures are based on the use of integral transforms, singular integral equations and Chebyshev polynomial expansions. Numerical calculations are carried out to show the effect of crack geometry, applied electric fields, electric boundary conditions along the crack faces, incident and reflecting waves on the time history of SIF and EDIF. The following conclusions may be drawn:

(1) For both the permeable and impermeable boundary conditions, the dynamic SIF history sees the continuous action of incident and reflecting waves. The time to reach its maximum varies with the geometry of the laminate and the wave speeds of materials.
(2) The influence of applied electric fields on the dynamic SIF history varies with time. When the action of electro-elastic waves is prevalent, the presence of an electric field may lead to the increase or decrease of SIF with increasing time, depending on the direction of the electric field and the loading process. When the action of elastic waves is prevalent, the effect of electric fields is negligible.
(3) For the case of the impermeable boundary condition, an overshoot phenomenon exists for the electric displacement intensity factor, and is intensified with the increase of crack length.
(4) The difference between the solutions of the permeable and impermeable electric boundary conditions is obvious. However, this difference is not as significant as it is usually thought to be.
(5) The interaction of cracks will lead to the increase of both the dynamic stress intensity factor and the electric displacement intensity factor.

## Acknowledgements

The financial support of this research by the Guangdong Provincial Natural Science Foundation and the Science Foundation of Shantou University is gratefully acknowledged.

## References

Chen, Z.T., Karihaloo, B.L., 1999. Dynamic response of a cracked piezoelectric ceramic under arbitrary electro-mechanical impact. International Journal of Solids and Structures 36, 5125–5133.

Chen, Z.T., Yu, S.W., 1997. Crack tip field of piezoelectric materials under anti-plane impact. Chinese Science Bulletin 42, 1613–1617.

Cheney, W., Kincaid, D., 1985. Numerical Mathematics and Computing, second ed. Brooks/Cole Publishing Company, Monterey.

Durbin, F., 1974. Numerical inversion of Laplace transforms: an efficient improvement to Duber and Abate's method. The Computer Journal 17, 371–376.

Li, S., Mataga, P.A., 1996a. Dynamic crack propagation in piezoelectric materials. Part 1: Electrode solution. Journal of the Mechanics and Physics of Solids 44, 1799–1830.

Li, S., Mataga, P.A., 1996b. Dynamic crack propagation in piezoelectric materials. Part 2: Vacuum solution. Journal of the Mechanics and Physics of Solids 44, 1831–1866.

Li, Y., Qi, D., 1979. Theory of Spline Functions. Academic Press, Beijing.

Meguid, S.A., Chen, Z.T., 2001. Transient response of a finite piezoelectric strip containing coplanar insulating cracks under electro-mechanical impact. Mechanics of Materials 33, 85–96.

Meguid, S.A., Wang, X.D., 1998. Dynamic anti-plane behavior of interacting cracks in a piezoelectric material. International Journal of Fracture 91, 391–403.

Meguid, S.A., Zhao, X., 2002. The interface crack problem of bonded piezoelectric and elastic half space under transient electro-mechanical loads. Journal of Applied Mechanics ASME 69, 244–253.

Narayanan, G.V., Beskos, D.E., 1982. Numerical operational methods for time-dependent linear problems. International Journal for Numerical Methods in Engineering 18, 1829–1854.

Narita, F., Shindo, Y., 1998. Dynamic anti-plane shear of a cracked piezoelectric ceramic. Theoretical and Applied Fracture Mechanics 29, 169–180.

Narita, F., Shindo, Y., 1999. Scattering of antiplane shear waves by a finite crack in piezoelectric laminates. Acta Mechanica 134, 27–43.

Shin, J.W., Kwon, S.M., Lee, K.Y., 2001. An eccentric crack in a piezoelectric strip under anti-plane shear impact loading. International Journal of Solids and Structures 38, 1483–1494.

Wang, X.D., 2001. On the dynamic behavior of interacting interfacial cracks in piezoelectric media. International Journal of Solids and Structures 38, 815–831.

Wang, X.D., Meguid, S.A., 2000. Modelling and analysis of the dynamic behaviour of piezoelectric materials containing interacting cracks. Mechanics of Materials 32, 723–737.

Wang, X., Yu, S., 2000. Transient response of a crack in a piezoelectric strip subjected to the mechanical and electrical impacts. International Journal of Solids and Structures 37, 5795–5808.

Wang, B.L., Han, J.C., Du, S.Y., 2000. Electroelastic fracture dynamics for multi-layered piezoelectric materials under dynamic anti-plane shearing. International Journal of Solids and Structures 37, 5219–5231.

Wen, P.H., Aliabadi, M.H., Rooke, D.P., 1996a. Dynamic analysis of mode III cracks in rectangular sheets. International Journal of Fracture 80, R37–R41.

Wen, P.H., Aliabadi, M.H., Rooke, D.P., 1996b. The influence of elastic waves on dynamic stress intensity factors (two dimensional problem). Archive of Applied Mechanics 66, 326–335.

Zhao X, Meguid, S.A., 2002. On the dynamic behaviour of a piezoelectric laminate with multiple interfacial collinear cracks. International Journal of Solids and Structures 39, 2477–2494.